JACS Au
AN OPEN ACCESS JOURNAL OF THE AMERICAN CHEMICAL SOCIETY

pubs.acs.org/jacsau
Article

Insulator-Based Dielectrophoresis for Purifying Semiconductor Industry-Compatible Chemicals with Trace Nanoparticles

Donggyu Lee,[#] Seungyun Lee,[#] Jinhyeok Jang, Jun Young Oh, Younghun Kim, Sam-Jong Choi, Yun Ho Kim,[*] and Jihyun Kim[*]

Cite This: *JACS Au* 2025, 5, 2342−2349
Read Online

ACCESS | Metrics & More | Article Recommendations | Supporting Information

ABSTRACT: As semiconductor scaling advances below 2−3 nm dimensions, precise control of nanoscale impurities becomes crucial for maintaining device performance and production yield. Conventional purification methods, such as distillation and filtration, are ineffective in removing nanoparticles smaller than 10 nm. This study investigates insulator-based dielectrophoresis (iDEP) for efficient removal of silica nanoparticles from semiconductor processing chemicals. Interdigitated electrode patterns fabricated on sapphire substrates were employed to generate high electric field gradients, facilitating nanoparticle aggregation. A 20 nm-thick aluminum oxide passivation layer was deposited via atomic layer deposition to prevent electrode degradation. Finite element method simulations confirmed that the strong electric field gradient necessary for nanoparticle aggregation was generated at the electrode edges. The optimal frequency for nanoparticle aggregation was determined using the Clausius−Mossotti factor, and large-scale iDEP experiments demonstrated a 41.3% reduction in Si concentration in deionized water and a 23.4% reduction in 2% nitric acid after 12 purification cycles. This method effectively removes the nanoparticles that are difficult to eliminate using conventional techniques, enhancing the purity of semiconductor processing chemicals. The study demonstrates iDEP's scalability, high throughput, and reliability for industrial applications, offering a promising solution for meeting purity standards in semiconductor fabrication.

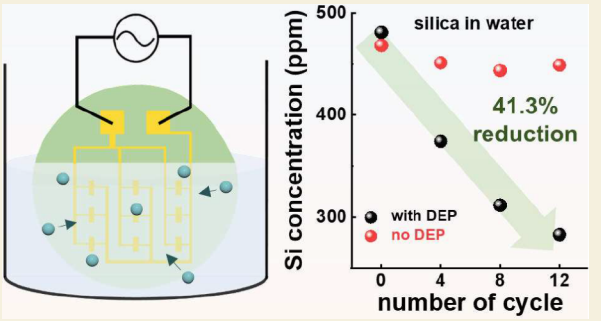

KEYWORDS: *dielectrophoresis, purification, semiconductor, manufacturing, nanoparticle, aggregation*

INTRODUCTION

As semiconductor miniaturization progresses to sub 2 nm nodes in logic devices, controlling nanoscale impurities has become increasingly critical for maintaining circuit integrity and performance.[1−3] These contaminants not only lower chip yield but also result in substantial financial losses in high-volume manufacturing. Ensuring the purity of chemicals used in semiconductor fabrication is essential for sustaining high production yields.[4] For instance, silicon impurities in chemicals can react with residues on wafers during cleaning, potentially inducing defects such as unintended SiGe epitaxial growth.[5] However, achieving ultrahigh purity at the nanoscale remains a critical challenge. While conventional purification methods such as distillation, filtration, and ion exchange effectively remove submicrometer-scale impurities, they are inadequate for capturing nanoscale contaminants. In particular, commercial filtration systems including membrane filtration often fail to achieve pore sizes small enough to capture particles below 10 nm.[6] These challenges required advanced purification technologies capable of efficiently removing nanoscale silicon impurities while remaining scalable for high-volume production.

Various nanoparticle manipulation techniques have been developed, including optoelectronic tweezers, optical trapping, magnetic control, and dielectrophoresis (DEP).[7−12] Among these, DEP has demonstrated high efficiency and scalability for nanoparticle manipulation, particularly in large-scale systems.[13−15] DEP induced the movement of polarizable particles in a nonuniform electric field through the interaction between induced dipoles and the electric field gradient.[16−18] This mechanism depends on the relative permittivity of the particle and the surrounding medium, which allows for its application to a wide range of materials, from biological cells to nanoscale particles.[13,19,20] However, a significant limitation of DEP is that the force exerted on a particle is proportional to its volume, significantly reducing its effectiveness for nanoparticles. To overcome this challenge, studies have focused on increasing the electric field gradient which directly influences the DEP

Received: March 17, 2025
Revised: May 7, 2025
Accepted: May 8, 2025
Published: May 15, 2025

https://doi.org/10.1021/jacsau.5c00307
JACS Au 2025, 5, 2342−2349

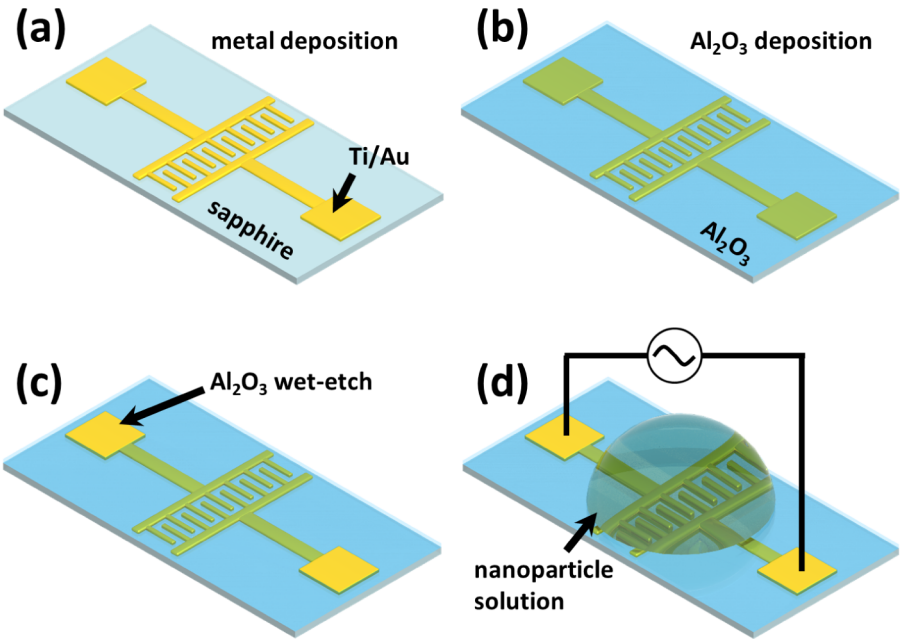

Figure 1. Fabrication and operation of the micropatterned iDEP device. (a) Ti/Au electrodes were defined to form the interdigitated iDEP electrodes. (b) A 20 nm-thick Al_2O_3 layer was deposited using the ALD process. (c) The Al_2O_3 layer on the contact pads was selectively wet-etched for AC biasing. (d) A solution containing silica nanoparticles was dropped on the iDEP device, followed by the application of a sinusoidal AC voltage.

force through interdigitated or sharp-tip configurations.[21,22] Purifying semiconductor chemicals for industrial applications requires a reusable large-scale system capable of efficiently removing nanoparticles. Such systems must also demonstrate reliable performance across various operational conditions, including both aqueous and acidic environments, ensuring versatility in industrial processes. DEP substrate can be reused by selectively removing aggregated particles, whereas conventional filtration methods require filter replacement.

In this study, we present an advanced purification method using insulator-based dielectrophoresis (iDEP) to aggregate and remove silica nanoparticles. High electric field gradients were generated by interdigitated electrode patterns on a sapphire substrate, facilitating efficient nanoparticle aggregation. An aluminum oxide (Al_2O_3) passivation layer was deposited via atomic layer deposition (ALD) to prevent electrode degradation and contamination during the DEP process. The Clausius−Mossotti (CM) factor was calculated to determine the optimal frequency range for silica nanoparticle aggregation at the edges of the interdigitated electrodes. Additionally, large-scale iDEP experiments were conducted repeatedly to evaluate the nanoparticle removal efficiency, with the aggregated particles subsequently cleaned using buffered oxide etchant (BOE). After 12 DEP cycles, Si concentration measurements showed a 41.3% reduction in deionized water (DIW) and a 23.4% reduction in 2% nitric acid. This approach successfully removed nanoparticles that conventional purification systems struggle to eliminate, significantly enhancing the purity of semiconductor processing chemicals.

RESULTS AND DISCUSSION

When particles are exposed to a nonuniform electric field, the DEP force arises from particle polarization, enabling their manipulation. The DEP force acting on a spheroidal particle suspended in a medium can be expressed as:

$$F_{DEP} = 2\pi\varepsilon_m R^3 \cdot Re\left(\frac{\varepsilon_p^* - \varepsilon_m^*}{\varepsilon_p^* + 2\varepsilon_m^*}\right)\cdot\nabla|E|^2 \quad (1)$$

where ε_m is the medium permittivity, R is the particle radius, ε_p^* and ε_m^* are the complex permittivities of the particle and medium, and $\nabla|E|^2$ is the gradient of the squared electric field magnitude.[23] The DEP force strongly depends on particle volume and decreases substantially with particle size.[24] At the nanoscale, the influence of Brownian motion becomes dominant over DEP forces, presenting significant challenges for nanoparticle manipulation.[25] Silica nanoparticles, common impurities in chemicals used for semiconductor manufacturing, typically range from a few nanometers to 100 nm. Their small size results in weak DEP forces, making their manipulation difficult. Polarizability, which indicates a particle's capacity to induce a dipole under an electric field, is crucial in determining the DEP behavior of a particle. Among various impurities, silica nanoparticles are particularly difficult to manipulate through DEP due to their low polarizability.[26] Particles with higher polarizability respond more effectively to electric fields, enhancing particle manipulation. The polarizability closely correlates with the relative permittivity of the particle, defined by the CM relation:

$$\frac{\varepsilon_r - 1}{\varepsilon_r + 2} = \frac{N\alpha}{3\varepsilon_0} \quad (2)$$

where ε_r denotes relative permittivity, N represents the number density of the molecules, α is the molecular polarizability, and ε_0 is the permittivity of free space.[27] A comparative analysis of silicon and silica nanoparticles, both common impurities in semiconductor manufacturing, reveals significant differences in their dielectric properties. Silicon nanoparticles with a relative permittivity of 11.7 exhibit strong polarization and high responsivity to electric fields.[28] In contrast, silica nanoparticles

https://doi.org/10.1021/jacsau.5c00307
JACS Au 2025, 5, 2342−2349

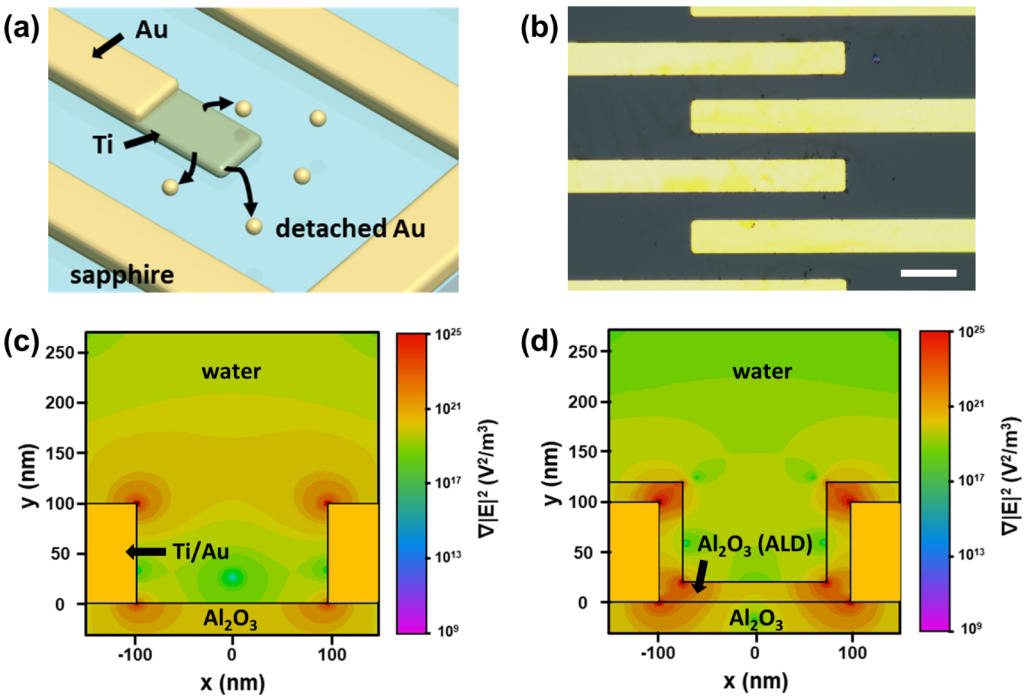

Figure 2. (a) Schematic of electrode degradation and subsequent solution recontamination. (b) Optical microscopy image of Ti/Au electrodes with a 20 nm-thick Al_2O_3 layer deposited via ALD (scale bar: 20 μm). An AC voltage frequency of 1 kHz and V_{pp} of 10 V is applied. Plots of the $\nabla|E|^2$ in a cross-sectional view (c) without and (d) with a 20 nm-thick Al_2O_3 layer, under a 10 V applied potential with a 200 nm electrode gap.

with a lower relative permittivity of 3.8 exhibit reduced polarizability, making their electrokinetic manipulation more challenging at the nanoscale.[20,29]

To address the challenges of manipulating silica impurities due to their nanosize and low polarizability, we enhanced the DEP force by intensifying the electric field gradient. Since the DEP force is proportional to $\nabla|E|^2$, reducing the electrode spacing to 10 μm significantly amplified the electric field gradient, enhancing the DEP force.[30] To implement this design, micropatterned interdigitated electrodes were fabricated on a sapphire substrate using photolithography, followed by Ti/Au deposition via e-beam evaporation (Figure 1a). This interdigitated design minimizes series resistance and maximizes edge exposure, improving nanoparticle trapping efficiency.[13] A 20 nm-thick Al_2O_3 passivation layer was then deposited using ALD (Figure 1b).[31] Contact pad areas were defined by photolithography, and the Al_2O_3 layer was selectively etched with phosphoric acid for electrical contacts between the Au probe tips and the contact pads of the device (Figure 1c). The significantly lower etch rates of Ti, Au, and SiO_2 compared to Al_2O_3 enabled selective etching. Following the etching process, the micropatterned electrodes were connected to a function generator via the probe station. The silica nanoparticle solution was carefully dropped onto the interdigitated electrode region while avoiding contact with the Au probe tips at the contact pads, and an alternating current (AC) voltage was then applied through the function generator (Figure 1d). To simulate semiconductor manufacturing conditions, Ludox colloidal silica was selected due to its particle size distribution, which is comparable to that observed in the manufacturing process. Analysis of the Ludox solution confirmed that the silica nanoparticles were smaller than 100 nm, with the highest distribution in the 7−10 nm range (Figure S1).

The micropatterned electrodes in the DEP chip generate highly localized electric fields, enabling effective modulation of silica nanoparticles. However, the application of an AC voltage to an unpassivated electrode leads to electrode degradation at the overlap regions of the interdigitated electrodes, where the electric field gradient is maximized (Figures 2a and S2).[32] This degradation results from the reduced interelectrode spacing, which increases the electric field gradient.[30] Under these high-electric field gradient conditions, Au atoms detach from the underlying Ti layer, disrupting the continuous transmission of AC signals and weakening the DEP forces acting on the target nanoparticles.[32] Furthermore, the detached Au atoms disperse into the solution due to direct electrode-medium contact, leading to solution contamination.

To address this electrode degradation, iDEP was employed, offering several advantages over conventional electrode-based DEP.[33] In iDEP systems, insulating structures are inserted between the electrodes and the medium, preventing direct contact between them. This configuration significantly reduces the electrode degradation and contamination issues commonly observed in conventional electrode-based DEP systems, where electrodes directly contact the medium. To achieve this, a 20 nm-thick Al_2O_3 passivation layer was deposited via ALD over the interdigitated electrodes. As demonstrated in Figure 2b, the Al_2O_3-passivated electrodes maintain their structural integrity even under intense electric field gradients, unlike unpassivated electrodes, which exhibit severe degradation. The passivation layer effectively prevents Au atom detachment, preserving DEP force generation throughout the operation. When a dielectric layer is used as a passivation layer, the AC electric field couples capacitively into the solution, influencing the movement of silica nanoparticles. Since the dielectric layer modifies the nonuniform electric field distribution between electrodes, investigating its effect on DEP force generation is necessary for effective particle manipulation. Finite element method (FEM) simulations were conducted to evaluate modifications in the electric field gradient induced by the passivation layer.

https://doi.org/10.1021/jacsau.5c00307
JACS Au 2025, 5, 2342−2349

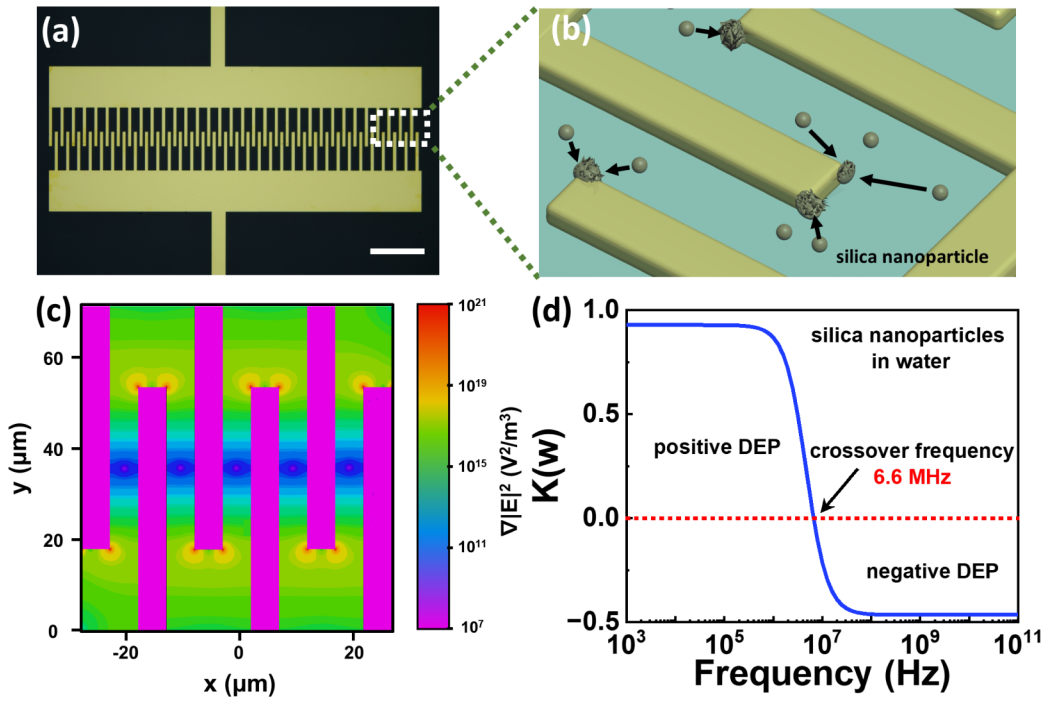

Figure 3. (a) Optical microscopy image of a micropatterned iDEP device (scale bar: 200 μm). (b) Silica nanoparticles trapped in regions with the strongest electric field gradient. (c) Magnitude plot of $\nabla|E|^2$ for a 10 V potential and 5 μm electrode spacing, highlighting a strong peak at the electrode edge. (d) CM factor plot for the silica nanoparticle in water at varying AC field frequencies.

The simulation domain consisted of DIW as the solvent for the silica nanoparticle solution, with a fixed potential difference of 10 V applied between electrodes, consistent with the experimental conditions. The simulation parameters are summarized in Table S1. Figure 2c shows the electric field gradient distribution between two electrodes without a passivation layer. Upon depositing a uniform 20 nm thick Al_2O_3 passivation layer, the modified electric field gradient distribution is depicted in Figure 2d. In both cases, the most intense electric field gradients are observed at the electrode edges, with intensity decreasing as the distance from these points increases. As the DEP force is proportional to $\nabla|E|^2$, silica nanoparticles experience the strongest DEP forces near the electrode edges, leading to their aggregation at these points. Furthermore, the magnitude of the applied electric field gradients remained consistent, regardless of the presence of the Al_2O_3 passivation layer (Figure S3). The micropatterned DEP device effectively manipulates silica nanoparticles by generating enhanced field gradients. However, for practical semiconductor manufacturing applications, the system must exhibit chemical resistance against acids to prevent solution recontamination during purification. Al_2O_3, selected as the passivation layer, provides excellent resistance to acidic chemicals commonly used in semiconductor manufacturing processes.[34] This highly chemical-resistant layer enhances both the stability of the DEP chip and its reliability in harsh manufacturing environments.

Figure 3a shows an optical microscopy image of the micropatterned iDEP device, where an AC voltage applied to interdigitated electrodes generates an electric field, manipulating the movement of silica nanoparticles. When the AC bias is applied, the $\nabla|E|^2$ reaches its maximum at the electrode edges, whereas the central regions of the overlapping electrode exhibit relatively lower field intensities, as depicted in Figure 3c. This spatial distribution of field intensity influences the behavior of polarizable particles suspended in the medium, causing their motion to depend on the frequency of the applied AC voltage. The direction and frequency dependence of the force acting on the particles is determined by the CM factor. For a spheroidal particle, the CM factor is expressed as

$$f_{CM}(\omega) = \frac{\varepsilon_p^*(\omega) - \varepsilon_m^*(\omega)}{\varepsilon_p^*(\omega) + 2\varepsilon_m^*(\omega)} \tag{3}$$

$$\varepsilon_p^*(\omega) = \varepsilon_p - i\frac{\sigma_p}{\omega}, \quad \varepsilon_m^*(\omega) = \varepsilon_m - i\frac{\sigma_m}{\omega} \tag{4}$$

where $\varepsilon_p(\sigma_p)$ and $\varepsilon_m(\sigma_m)$ are the electrical permittivity (conductivity) of the particle and medium, respectively, i is the imaginary unit, and ω is the angular frequency of the AC voltage.[35] To investigate the frequency-dependent behavior of silica nanoparticles (conductivity = 0.04 S/m) in DIW (conductivity = 10 S/m), the real part of the CM factor was plotted as a function of the frequency (Figure 3d).[29] The crossover frequency, where the CM factor becomes zero, is observed at 6.6 MHz. Below this frequency, a positive CM factor corresponds to a positive DEP (p-DEP) behavior, where polarized silica particles migrate toward regions of stronger electric field gradients. Conversely, the negative CM factor at frequencies above 6.6 MHz indicates negative DEP (n-DEP), where silica particles move toward regions of weaker electric field gradients. Under p-DEP conditions, silica particles accumulate at the electrode edges, where $\nabla|E|^2$ is most intense, resulting in dense silica aggregates (Figure 3b).

Based on these theoretical predictions, we experimentally investigated the frequency-dependent manipulation characteristics of silica nanoparticles. Figure 4a presents the frequency-dependent nanoparticle behavior at the iDEP electrode edges at frequencies of 100 kHz, 1 MHz, and 80 MHz. As indicated by the CM factor analysis (Figure 3d), frequencies below the crossover frequency of 6.6 MHz correspond to the p-DEP

https://doi.org/10.1021/jacsau.5c00307
JACS Au 2025, 5, 2342−2349

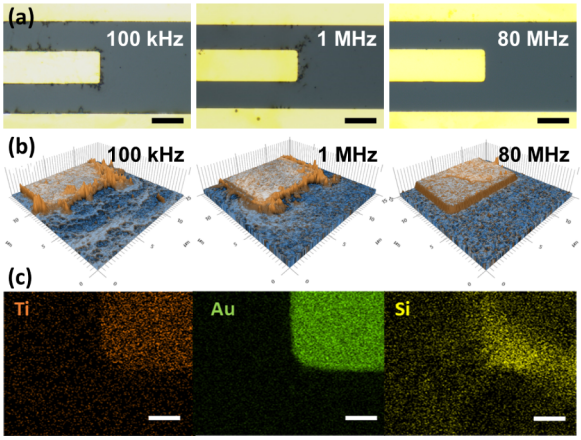

Figure 4. Frequency-dependent DEP manipulation of silica nanoparticles suspended in DIW. (a) Optical microscopy images (scale bar: 10 μm), and (b) 3D AFM mappings of the electrode edges after iDEP at 100 kHz, 1 MHz, and 80 MHz. The iDEP was conducted at an 10 V_{pp} of 10 V for 20 min. (c) EDS elemental maps (Ti, Au, and Si) of the electrode edges after DEP manipulation for 20 min (scale bar: 1 μm).

regime, where silica nanoparticles migrate toward regions with high electric field gradients. When exposed to peak-to-peak voltage (V_{pp}) of 10 V at 100 kHz for 20 min, silica aggregates formed at the electrode edges, as shown in Figure 4a. A similar aggregation pattern was observed at 1 MHz, as both 100 kHz and 1 MHz fall within p-DEP regime. Furthermore, the extent of nanoparticle aggregation at the electrode edges increased with longer DEP process durations (Figures S4 and S5). After 20 min, silica nanoparticles fully aggregated in the regions with a high electric field gradient, and no further aggregation was observed during subsequent processes. Conversely, at frequencies above the crossover frequency of 6.6 MHz, n-DEP behavior dominates. At 80 MHz, the silica nanoparticles were repelled from the electrode edges due to n-DEP behavior, resulting in the absence of observable aggregation.

To quantitatively characterize the aggregated silica nanoparticles, atomic force microscopy (AFM) measurements were conducted. Figure 4b presents 3D AFM mappings of the electrode edge with various frequencies. Consistent with the optical microscopy observations, silica nanoparticles aggregated at the electrode edges at frequencies below the crossover frequency. The surface roughness in these regions was analyzed using the root-mean-square method, calculated with the equation below:

$$R_q = \sqrt{\frac{1}{l_r}\int_0^{l_r} z(x)^2 dx} \tag{5}$$

where l_r represents the length of the mean line, and $z(x)$ denotes the difference from the average height at each measured point on the surface. Surface roughness measurements yielded 57.5 nm at 100 kHz, 57.2 nm at 1 MHz, and 3.5 nm at 80 MHz, which confirm significant nanoparticle aggregation at frequencies that exhibit p-DEP behavior. AFM height profiles were examined to perform a more detailed size analysis of the aggregated nanoparticles (Figure S6). The average heights were measured as 119.4 nm at 100 kHz and 110.8 nm at 1 MHz. Given the size of the pristine silica nanoparticles, these results further support the aggregation of particles under both frequency conditions (Figure S1). Additionally, to confirm the elemental composition of the aggregates near the interdigitated electrodes, energy-dispersive X-ray spectroscopy (EDS) analysis was conducted (Figure 4c). Comparison with EDS data from electrodes without the DEP process revealed increased Si concentrations around the electrodes, confirming the presence of silica aggregates (Figure S7).

In addition to the DEP chip-based studies, large-scale experiments were conducted to validate the nanoparticle aggregation and removal from the solution. Large-scale iDEP experiments utilizing a 2 in. substrate were performed to quantify the removal efficiency of silica nanoparticles in solution. Figure 5a shows an image of the 2 in. sapphire substrate, which incorporates 36 interdigitated patterns and two large contact pads designed for function generator connections. Each contact pad is connected to the left and right sides of the interdigitated patterns, with the Al_2O_3 passivation layer selectively etched in the contact pad areas to enable electrical contact with the Au tips. To ensure effective operation, the large-scale iDEP substrate was immersed vertically in the solution while keeping the contact pads above the solution level, as illustrated in Figure S8. During each 20 min DEP cycle, silica nanoparticles aggregated at the edges of the interdigitated electrodes, decreasing their concentration in the solution. However, the accumulation of nanoparticles at the electrode edges gradually reduced the removal efficiency over subsequent cycles. To ensure consistent performance, the aggregated silica nanoparticles were removed with BOE for 10 s after each DEP cycle. The selective etching properties of BOE effectively removed the silica particles while preserving the integrity of the Al_2O_3 passivation layer. The 20 nm-thick Al_2O_3 layer also prevented

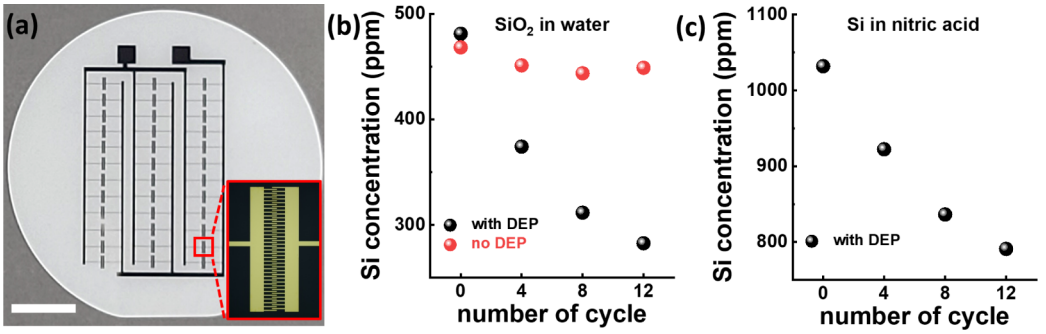

Figure 5. Removal of silica nanoparticles via large-scale iDEP. (a) Photograph of a 2 in. sapphire substrate featuring 36 interdigitated DEP patterns (scale bar: 1 cm). Si concentration at different iDEP cycles in (b) DIW and (c) 2% nitric acid, comparisons with and without DEP process.

https://doi.org/10.1021/jacsau.5c00307
JACS Au 2025, 5, 2342−2349

electrode detachment, ensuring the reusability of the substrate across multiple DEP cycles.

While the iDEP chip experiments were conducted at a frequency of 100 kHz for optimal p-DEP, the large-scale iDEP design required frequency adjustment due to the increased distance between the contact pads and the interdigitated patterns. This extended distance limited the effective application of AC voltage at 100 kHz, necessitating operation at a lowered frequency of 1 kHz to achieve a uniform field distribution across all interdigitated patterns. Additionally, a DIW solution with Si concentration of approximately 500 ppm was prepared to simulate actual conditions, reflecting the impurity concentrations typically found in chemicals used in the semiconductor industry. To evaluate the removal efficiency, 12 DEP cycles were conducted, each followed by substrate cleaning with BOE. The Si concentration in the solution was monitored using inductively coupled plasma atomic emission spectroscopy (ICP-AES) during the DEP process (Figure 5b). ICP-AES measurements were repeated three times for each cycle, and the average Si concentration was used for analysis. Since silica nanoparticles were the only Si-based compound in the solution, the measured Si concentration directly corresponded to the concentration of silica nanoparticles. After 12 DEP cycles, the Si concentration decreased by 41.3%, confirming the effective removal of silica nanoparticles from the solution.

Control experiments were conducted by repeatedly immersing the DEP substrate for 20 min without applying an electric field. These control experiments showed negligible changes in Si concentration, indicating that particle removal was exclusively driven by the DEP process. The raw data of Si concentration, both with and without DEP cycles, are summarized in Table S2. To further validate the nanoparticle removal under acidic conditions, large-scale iDEP experiments were conducted using an ICP standard solution containing silicon nanoparticles in 2% nitric acid. The Si concentration decreased gradually throughout the DEP process, exhibiting trends similar to those observed with DIW (Figure 5c). A 23.4% reduction in Si concentration was achieved after 12 DEP cycles, while control experiments demonstrated minimal changes, further validating the effectiveness of DEP-based removal. The stability of the Al_2O_3 passivation layer was also verified by consistent Al concentrations throughout the DEP process (Figure S9). The Al concentration remained stable at approximately 1 ppm across all DEP cycles, confirming that neither the DEP process nor the BOE treatment affected the Al_2O_3 passivation layer or substrate.

CONCLUSIONS

This study demonstrates that iDEP provides an effective and scalable approach for removing silica and silicon nanoparticles, common impurities in semiconductor manufacturing, from both acidic and DIW solutions. The introduction of a 20 nm-thick Al_2O_3 passivation layer successfully protected the iDEP electrodes from degradation in acidic environments without affecting nanoparticle aggregation. Both theoretical and experimental analyses validated that the iDEP process effectively manipulates nanoparticles in the solutions through enhanced electric field gradients at optimal frequencies. Large-scale (2 in.) iDEP experiments resulted in a 41.3% reduction in Si concentration after 12 purification cycles, revealing both scalability and purification efficiency for industrial applications. Additionally, the iDEP system achieved a 23.4% reduction in Si concentration in acidic solutions, confirming its effectiveness across diverse chemical environments. These findings highlight the advantages of iDEP over conventional purification methods, including its high throughput, operational reliability, and adaptability to various chemical environments. This technology presents a promising solution for enhancing semiconductor manufacturing yield and efficiency by meeting increased contamination control standards.

EXPERIMENTAL SECTION

Device Fabrication

The sapphire pieces (1.5 cm × 1.5 cm) for the DEP chip and the 2 in. sapphire substrates for large-scale iDEP were initially cleaned with acetone and isopropyl alcohol. Subsequently, LOR 5A and AZ GXR-601 photoresists were spin-coated onto the sapphire substrates. Micro-DEP electrodes were then patterned using photolithography (DL-1000A1, Nano System Solutions), followed by the deposition of Ti/Au (20/80 nm) via e-beam evaporation. To passivate the electrodes, a 20 nm-thick Al_2O_3 layer was deposited at 200 °C using ALD. The Al_2O_3 layer on the contact pads was selectively removed by photolithography and wet etching with phosphoric acid for 60 s, exposing the contact pads.

DEP Experiments

A colloidal silica nanoparticle solution (LUDOX SM, Grace) diluted with DIW was used in the DEP experiments. For the DEP chip experiments, the nanoparticle solution was dropped on the interdigitated electrodes, and the contact pads were connected to a function generator (33250A, Agilent) via a probe station. A sinusoidal bias with V_{pp} of 10 V was applied, and the frequency was varied from 1 kHz to 80 MHz. After the DEP process, the residual solution was removed with N_2 blowing. For the large-scale iDEP experiments, the fabricated 2 in. sapphire substrates for iDEP were vertically immersed in the solution to prevent the contact pads from being submerged in the solution. The contact pads were connected to a function generator, and V_{pp} of 10 V at 1 kHz was applied to induce particle aggregation. After the iDEP process, the substrate was immersed in BOE solution to remove the aggregated particles. For experiments in acidic solutions, Si standard solution (Silicon Standard for ICP, Sigma-Aldrich) was used. After rinsing with DIW, the substrates were dried with nitrogen gas. This process was repeated multiple times to validate the consistency and efficiency of nanoparticle removal.

Characterization

Optical microscopy was employed to analyze the morphology of the samples. The morphology of concentrated silica aggregates around the electrode edges was further analyzed by scanning electron microscopy (SEM; GeminiSEM 560, ZEISS) at the National Center for Interuniversity Research Facilities (NCIRF) at Seoul National University. EDS was conducted to confirm that the aggregates observed on the electrode edges consisted of silica. The size of the aggregated particles formed during the DEP process and the roughness of the surrounding areas were examined using AFM (NX10, Park Systems). The size distribution of silica nanoparticles in the solution was measured with a Zetasizer (Nano ZS, Malvern Panalytical). ICP-AES (ICPS-8100, Shimadzu) was used to determine the concentration of silica nanoparticles in the solution.

ASSOCIATED CONTENT

Supporting Information

The Supporting Information is available free of charge at https://pubs.acs.org/doi/10.1021/jacsau.5c00307.

Atomic number percentage distribution of nanoparticles, optical microscopy image, 3D simulation plot, AFM data, elemental distribution maps, Al concentration plot, and simulation parameters (PDF)

https://doi.org/10.1021/jacsau.5c00307
JACS Au 2025, 5, 2342−2349

AUTHOR INFORMATION

Corresponding Authors

Yun Ho Kim − *Material Technology Team, Common Technology Center, DS, Samsung Electronics, Suwon, Gyeonggi-do 17786, Republic of Korea*; Email: yunho17.kim@samsung.com

Jihyun Kim − *Department of Chemical and Biological Engineering, Seoul National University, Seoul 08826, Republic of Korea*; orcid.org/0000-0002-5634-8394; Email: jihyunkim@snu.ac.kr

Authors

Donggyu Lee − *Department of Chemical and Biological Engineering, Seoul National University, Seoul 08826, Republic of Korea*; orcid.org/0009-0009-8099-3578

Seungyun Lee − *Department of Chemical and Biological Engineering, Seoul National University, Seoul 08826, Republic of Korea*; orcid.org/0009-0001-9609-5424

Jinhyeok Jang − *Material Technology Team, Common Technology Center, DS, Samsung Electronics, Suwon, Gyeonggi-do 17786, Republic of Korea*

Jun Young Oh − *Material Technology Team, Common Technology Center, DS, Samsung Electronics, Suwon, Gyeonggi-do 17786, Republic of Korea*

Younghun Kim − *Material Technology Team, Common Technology Center, DS, Samsung Electronics, Suwon, Gyeonggi-do 17786, Republic of Korea*

Sam-Jong Choi − *Material Technology Team, Common Technology Center, DS, Samsung Electronics, Suwon, Gyeonggi-do 17786, Republic of Korea*

Complete contact information is available at: https://pubs.acs.org/10.1021/jacsau.5c00307

Author Contributions

#D.L. and S.L. contributed equally to this work. CrediT: D.L.: Writing—original draft, conceptualization, and methodology. S.L.: Writing—original draft, conceptualization, and methodology. J.J.: investigation and validation. J.Y.O.: investigation and validation. Y.K.: investigation and validation. S.-J.C.: project administration and supervision. Y.H.K.: project administration and supervision. J.K.: project administration, supervision, writing—review and editing, and conceptualization.

Notes

The authors declare no competing financial interest.

ACKNOWLEDGMENTS

This work was supported by Samsung Electronics Co., Ltd. (IO241021-11036-01) and the Technology Innovation Program (Development of plasma etching process using low GWP HFC gases, RS-2023-00267003) funded by the Ministry of Trade, Industry & Energy (MOTIE, Korea).

REFERENCES

(1) Jacob, A. P.; Xie, R.; Sung, M. G.; Liebmann, L.; Lee, R. T. P.; Taylor, B. Scaling Challenges for Advanced CMOS Devices. *Int. J. High Speed Electron. Syst.* **2017**, *26* (1n02), 1740001.

(2) Salahuddin, S.; Datta, K.; Ni, S. The era of hyper-scaling in electronics. *Nat. Electron.* **2018**, *1* (8), 442−450.

(3) Ratnesh, R. K.; Goel, A.; Kaushik, G.; Garg, H.; Prasad, M.; Singh, B.; Prasad, B. Advancement and challenges in MOSFET scaling. *Mater. Sci. Semicond. Process* **2021**, *134*, 106002.

(4) Okorn-Schmidt, H. F.; Holsteyns, F.; Lippert, A.; Mui, D.; Kawaguchi, M.; Lechner, C.; Frommhold, P. E.; Nowak, T.; Reuter, F.; Piqué, M. B. Particle Cleaning Technologies to Meet Advanced Semiconductor Device Process Requirements. *ECS J. Solid State Sci. Technol.* **2013**, *3* (1), 3069−3080.

(5) Yu, K.; Gaddam, S.; Bhattacharyya, D.Reduction of Streak Signature of SiGe Epitaxial Unwanted Growth by Pre-cleaning Process Recipe Optimization*2023 34th Annual SEMI Advanced Semiconductor Manufacturing Conference (ASMC). IEEE*20231−4

(6) Juo, J.; Qiao, R.; Ding, B. Enhancement of ion selectivity and permeability in two-dimensional material membranes. *Matter* **2024**, *7* (10), 3351.

(7) Zhang, S.; Juvert, J.; Cooper, J. M.; Neale, S. L. Manipulating and assembling metallic beads with Optoelectronic Tweezers. *Sci. Rep.* **2016**, *6* (1), 32840.

(8) Zhang, Y.; Min, C.; Dou, X.; Wang, X.; Urbach, H. P.; Somekh, M. G.; Yuan, X. Plasmonic tweezers: for nanoscale optical trapping and beyond. *Light: sci. Appl.* **2021**, *10* (1), 59.

(9) Singh, K. K.; Kumar, D.; Singh, A.; Goswami, D. Precise Nanoparticle Manipulation Using Femtosecond Laser Trapping. *J. Phys. Chem. Lett.* **2024**, *15* (41), 10360−10365.

(10) Lee, D.; Lee, D.; Lee, S.; Park, H. J.; Han, K. N.; Choi, S. J.; Kim, Y. H.; Kim, J. Electric Field-Assisted Agglomeration of Trace Nanoparticle Impurities for Ultrahigh Purity Chemicals. *JACS Au.* **2024**, *4* (3), 1031−1038.

(11) Liu, M.; Yang, M.; Wan, X.; Tang, Z.; Jiang, L.; Wang, S. From Nanoscopic to Macroscopic Materials by Stimuli-Responsive Nanoparticle Aggregation. *Adv. Mater.* **2023**, *35* (20), 2208995.

(12) Tian, S.; Chen, X.; Ding, B. Manipulation of Single Nanowire and its Applications. *Small Methods* **2025**, 2402053.

(13) Barik, A.; Zhang, Y.; Grassi, R.; Nadappuram, B. P.; Edel, J. B.; Low, T.; Koester, S. J.; Oh, S. H. Graphene-edge dielectrophoretic tweezers for trapping of biomolecules. *Nat. Commun.* **2017**, *8* (1), 1867.

(14) Zavatski, S.; Martin, O. J. F. Visual and Quantitative Analysis of the Trapping Volume in Dielectrophoresis of Nanoparticles. *Nano Lett.* **2024**, *24* (33), 10305−10312.

(15) Sarno, B.; Heineck, D.; Heller, M. J.; Ibsen, S. D. Dielectrophoresis: Developments and applications from 2010 to 2020. *Electrophoresis* **2021**, *42* (5), 539−564.

(16) Constantinou, M.; Rigas, G. P.; Castro, F. A.; Stolojan, V.; Hoettges, K. F.; Hughes, M. P.; Adkins, E.; Korgel, B. A.; Shkunov, M. Simultaneous Tunable Selection and Self-Assembly of Si Nanowires from Heterogeneous Feedstock. *ACS Nano* **2016**, *10* (4), 4384−4394.

(17) Lan, M.; Yang, F. Applications of dielectrophoresis in microfluidic-based exosome separation and detection. *Chem. Eng. J.* **2024**, *491*, 152067.

(18) Gascoyne, P. R. C.; Vykoukal, J. Particle separation by dielectrophoresis. *Electrophoresis* **2002**, *23* (13), 1973−1983.

(19) Rezanoor, W.; Dutta, P. Combined AC electroosmosis and dielectrophoresis for controlled rotation of microparticles. *Biomicrofluidics* **2016**, *10* (2), 024101.

(20) Honegger, T.; Berton, K.; Picard, E.; Peyrade, D. Determination of Clausius−Mossotti factors and surface capacitances for colloidal particles. *Appl. Phys. Lett.* **2011**, *98* (18), 181906.

(21) Sadeghian, H.; Hojjat, Y.; Soleimani, M. Interdigitated electrode design and optimization for dielectrophoresis cell separation actuators. *J. Electrostatics* **2017**, *86*, 41−49.

(22) Jose, J.; Kress, S.; Barik, A.; Otto, L. M.; Shaver, J.; Johnson, T. W.; Lapin, Z. J.; Bharadwaj, P.; Novotny, L.; Oh, S. H. Individual Template-Stripped Conductive Gold Pyramids for Tip-Enhanced Dielectrophoresis. *ACS Photonics* **2014**, *1* (5), 464−470.

(23) Çetin, B.; Li, D. Dielectrophoresis in microfluidics technology. *Electrophoresis* **2011**, *32* (18), 2410−2427.

(24) Kadaksham, A. T. J.; Singh, P.; Aubry, N. Dielectrophoresis of nanoparticles. *Electrophoresis* **2004**, *25* (21−22), 3625−3632.

(25) Jung, S. H.; Chen, C.; Cha, S. H.; Yeom, B.; Bahng, J. H.; Srivastava, S.; Zhu, J.; Yang, M.; Liu, S.; Kotov, N. A. Spontaneous Self-Organization Enables Dielectrophoresis of Small Nanoparticles

and Formation of Photoconductive Microbridges. *J. Am. Chem. Soc.* **2011**, *133* (28), 10688−10691.
(26) Robertson, J. High dielectric constant oxides. *Eur. Phys. J. Appl. Phys* **2004**, *28* (3), 265−291.
(27) Talebian, E.; Talebian, M. A general review on the derivation of Clausius−Mossotti relation. *Optik* **2013**, *124* (16), 2324−2326.
(28) Liberal, I.; Mahmoud, A. M.; Engheta, N. Geometry-invariant resonant cavities. *Nat. Commun.* **2016**, *7* (1), 10989.
(29) Chai, Z.; Yilmaz, C.; Busnaina, A. A.; Lissandrello, C. A.; Carter, D. J. Directed assembly-based printing of homogeneous and hybrid nanorods using dielectrophoresis. *Nanotechnology* **2017**, *28* (47), 475303.
(30) Nguyen, T. H.; Nguyen, H. T.; Ngo, N. A.; Nguyen, M. C.; Thu, H. B.; Ducrée, J.; Duc, T. C.; Bui, T. T.; Quang, L. D. Numerical study on a facing electrode configuration dielectrophoresis microfluidic system for efficient biological cell separation. *Sci. Rep.* **2024**, *14* (1), 27627.
(31) Levy, P.; Bianconi, M.; Correra, L. Wet Etching of Al_2O_3 for Selective Patterning of Microstructures Using Ar^+ Ion Implantation and H_3PO_4. *J. Electrochem. Soc.* **1998**, *145* (1), 344.
(32) Heineck, D. P.; Sarno, B.; Kim, S.; Heller, M. Electrochemical attack and corrosion of platinum electrodes in dielectrophoretic diagnostic devices. *Anal. Bioanal. Chem.* **2020**, *412*, 3871−3880.
(33) Lapizco-Encinas, B. H. On the recent developments of insulator-based dielectrophoresis: A review. *Electrophoresis* **2019**, *40* (3), 358−375.
(34) Naumann, V.; Otto, M.; Wehrspohn, R. B.; Hagendorf, C. Chemical and structural study of electrically passivating Al_2O_3/Si interfaces prepared by atomic layer deposition. *J. Vac. Sci. Technol., A* **2012**, *30* (4), 04D106.
(35) Pethig, R. Dielectrophoresis: Status of the theory, technology, and applications. *Biomicrofluidics* **2010**, *4* (2), 022811.

https://doi.org/10.1021/jacsau.5c00307
JACS Au 2025, 5, 2342−2349